ELSEVIER

Journal of Molecular Structure (Theochem) 681 (2004) 27–40

THEO CHEM

www.elsevier.com/locate/theochem

The onset of dissociation in the aqueous LiOH clusters: a solvation study with the effective fragment potential model and quantum mechanics methods

Akihiko Yoshikawa, Jorge A. Morales*

Department of Chemistry and Biochemistry, Texas Tech University, P.O. Box 41061, Lubbock, TX 79409-1061, USA

Received 23 February 2004; revised 11 April 2004; accepted 22 April 2004

Available online 7 June 2004

Abstract

The first systematic study on the solvation of the $LiOH(H_2O)_n$ ($n = 1–6, 8$) clusters is herein presented by using both the molecular-mechanics effective fragment potential (EFP) model and full quantum mechanics methods. Aqueous clusters are sequentially calculated first with the LiOH solute molecule described by a restricted Hartree–Fock (RHF) wavefunction and the H_2O solvent molecules by the EFP model (EFP/RHF), and then with the full quantum mechanics RHF and Møller–Pleset second-order perturbation (MP2) theories. Calculated properties include equilibrium geometries, Mulliken charges, bond lengths and orders, and relative energies inter alia. Present results indicate that at the least six H_2O molecules are necessary to be added to one LiOH molecule to cause its spontaneous dissociation into a Li^+/OH^- separated ion pair. Another instance of dissociation is also observed in one of the $LiOH(H_2O)_8$ isomers. EFP/RHF reasonably reproduces RHF structural properties and dissociation patterns but discrepancies arise in the solute charge description. Comparisons of the present theoretical results with previous EFP studies and with a few experimental data are also discussed.

Keywords: Effective fragment potential model; Solvation effects; Spontaneous dissociation of ionic compounds in aqueous clusters; Charge transfer

1. Introduction

In recent years, there has been a renovated interest in studying dissolution mechanisms and solvation effects by both modern experimental techniques and accurate computational methods [1]. The importance of those investigations can be readily seen by simply recalling the essential role played by solvation in the vast majority of chemical processes. Although the main features of dissolution and solvation are routine topics in chemistry textbooks, many microscopy details of those phenomena still remain uncertain. Fortunately, the emergence of more precise experimental techniques and the incessant growth in computational power are making possible very meticulous studies on dissolution and solvation at the molecular level. For instance, it has been recently established experimentally that the first primary hydration shells of the $OH^-(H_2O)_n$ and $F^-(H_2O)_n$ clusters in the gas phase do consist of exactly three and four H_2O molecules ($n = 3$ and 4), respectively [2]; and the first genuine, primary-shell, hexa-coordinated Na^+ cluster in the gas phase has been also recently synthesized and detected [3].

Although dissolution and solvation take places in bulk phase, the investigation of microscopic processes in a solution sample may become experimentally difficult and computationally costly. Therefore, a feasible approach to investigate solvation is to deal with individual clusters of one solute molecule coordinated with a few solvent molecules in the gas phase. This approach is so advantageous that even valid inferences about the solvation processes involving the Na^+ and K^+ ions in channel proteins have been drawn in that way [4]. The step-wise addition of solvent molecules to a bare solute in a cluster, via either experiments or computer simulations, can certainly reveal the minute details of dissolution and solvation and record the evolution of the system properties from a single and isolated molecule of solute to the bulk phase.

In the context of a theoretical investigation on solvation, an active field of research is the prediction of the minimum

* Corresponding author. Tel.: +1-806-742-3094; fax: +1-806-742-1289.
E-mail address: jorge.morales@ttu.edu (J.A. Morales).

0166-1280/$ - see front matter © 2004 Elsevier B.V. All rights reserved.
doi:10.1016/j.theochem.2004.04.047

number of H_2O molecules necessary to cause the dissociation of a single, isolated molecule of a strong acid [1], a strong hydroxide [5], or an ionic salt [6]. In a dilute aqueous solution of those species, one cation and one anion from the binary solute can form an ion pair that is coordinated by a few H_2O molecules. Two clearly distinct types of ion pairs can occur in a strong electrolyte solution: the separated ion pair and the contact ion pair, respectively. In a separated ion pair, the distance between the two ions is appreciably larger than their corresponding bond length in the isolated solute molecule in the gas phase. On the other hand, in a contact ion pair, the ions separation remains relatively close to that gas-phase bond length even when the pair is coordinated with a few H_2O molecules. The appearance of a genuine separated ion pair signals the onset of the solute dissociation in the solvent environment. Much of the theoretical analysis on aqueous solvation and ion-pair formation has been devoted to study strong electrolytes bearing Na^+ and Cl^- ions such as NaCl [6–12], HCl [13–22] and NaOH [5] inter alia. For instance, in a recent study, Jungwirth [6] has theoretically predicted the formation of a Na^+/Cl^- separated ion pair exhibiting a Na–Cl separation of 4.43 Å in the isolated $NaCl(H_2O)_6$ cluster by using Møller–Pleset second-order perturbation theory (MP2). This particular solvation environment for the formation of a Na^+/Cl^- separated ion pair is not surprising because the $NaCl(H_2O)_6$ cluster with a prism shape presents a balanced, three-dimensional, cage structure. In an interesting series of studies, Yoshikawa and Gordon [5] have also recently investigated the appearance of both separated and contact ion pairs for single NaOH and NaCl molecules solvated with up to six H_2O molecules. These authors could theoretically predicted that genuine Na^+/OH^- and Na^+/Cl^- separated ion pairs are formed in the $NaOH(H_2O)_6$ and $HCl(H_2O)_6$ clusters, exhibiting large ion separations of 4.15 and 4.00 Å; 4.03 and 4.65 Å; and 4.36 and 4.38 Å, at the levels of the effective fragmented potential (EFP), restricted Hartree–Fock (RHF), and MP2 theories, respectively [5].

Although studies on the aqueous solvation of several Na^+ compounds [6–12] have been conducted at length, there are comparatively far fewer experimental and computational studies on the solvation of Li^+ compounds [9,11,23,24]. The present investigation is therefore the first systematic theoretical study on the solvation of the strong LiOH base in the presence of up to eight H_2O molecules. The motivations for investigating such a particular system are diverse. First of all, any systematic study on solvation involving the alkali-metal ions should include the whole series of those ions in order to explain how the ions size and electronic configurations affect the solvation processes [4,5,24]. In that context, it will be of particular interest to compare the microscopic behavior of a LiOH molecule in an aqueous cluster with that of the most common NaOH in order to explain the different macroscopic properties of these two bases in bulk solution (e.g. the lower solubility of LiOH in H_2O). Another reason to investigate Li^+ compounds is that this ion has the smallest number of electrons in the series of alkali-metal ions, a circumstance that would make the simulation of large $(LiOH)_m(H_2O)_n$ clusters less computationally costly. It is also worth noticing that the current use of the moderately water-soluble Li_2CO_3 salt in the clinical treatment of bipolar disorder may trigger several theoretical investigations on the solvation and coordination of the Li^+ ion in order to reveal the still unknown mode of action of this ion in the brain system [25].

The ideal approach for a solvation study on a solute–solvent cluster would be a full ab initio calculation in which the entire system, solute and solvent, is treated as a supermolecule at a high-level theoretical method. However, such a type of calculation is computationally very expensive and can eventually become unfeasible. As long as the number of solvent molecules increases so does the size of the basis set used and so does the number of expected local minima on the potential energy surface. Therefore, a full ab initio approach is only practical in systems with a small number of solvent molecules. A way around this limitation is to employ a mixed quantum/classical (Q/C) method, where the solute molecule is described by an ab initio wavefunction, whereas the solvent molecules are treated by a less expensive molecular-mechanics (MM) type of model such as the effective fragment potential (EFP) model [5,7, 22,24]. EFP has been successfully applied to study numerous solvation processes in aqueous solutions involving NaCl [5,7], NaOH [5], alkali metal and alkaline-earth metal cation–water clusters $M^{+n}(H_2O)_{1-6}$ ($M^{+n} = Li^+$, Na^+, K^+, Mg^{2+} and Ca^{2+}) [24], anion–water clusters $A^-(H_2O)_{1-6}$ ($A^- = OH^-$, F^-, SH^-, Cl^- and Br^-) [26], oxyanion–water clusters $A^-(H_2O)_{1-4}$ ($A^- = ClO_4^-$, HSO_4^-, NO_3^-, $H_2PO_4^-$, HCO_3^-, HCO_2^-, SO_4^{2-}, HPO_4^{2-}, CO_3^{-2} and PO_4^{3-}) [27], and the amino acid glycine [28, 29], inter alia. In particular, the systematic EFP and ab initio investigations by Merrill, Webb and co-workers in Refs. [24,26] are highly relevant to the present study because they included the cases of the $Li^+(H_2O)_{1-6}$ [24] and $OH^-(H_2O)_{1-6}$ [26] ions that are the products of the complete dissociation of LiOH in water, respectively. Comparisons of our present results on the $LiOH(H_2O)_n$ ($n = 1–6, 8$) clusters with those on the $Li^+(H_2O)_{1-6}$ and $OH^-(H_2O)_{1-6}$ ions by Merrill et al. [24, 26] will be discussed in Section 3.2.

The present work reports the first systematic study of the effects of adding up to eight H_2O molecules to a single LiOH molecule by both a mixed Q/C, ab initio/EFP [22] model treatment of the solute/solvent system and also by full ab initio descriptions of the whole solute–solvent supermolecule, respectively. In the mixed Q/C, ab initio/ EFP approach, the quantum solute will be described at the level of the RHF theory (EFP/RHF), whereas in the full quantum treatments, the solute–solvent supermolecule will be calculated at both the RHF and MP2 levels of theory. An important aspect of the present study will be to attest

the ability of the EFP/RHF method to correctly predict the structural properties of both contact and separated ion pairs in comparison with the full ab initio methods.

2. Method and computation details

The EFP method has been explained in full detail in several papers [22] so that it will be briefly described herein. The EFP model was specifically developed to describe weak intermolecular interactions between a quantum mechanical solute and a molecular-mechanics solvent, where the latter is represented by an effective fragment potential. The model also includes the proper interactions among the different fragments. In the case of solute–fragment interactions, a one-electron term is incorporated into the ab initio Hamiltonian of the solute containing the Coulombic, polarization and exchange-repulsion/charge-transfer interactions, respectively. For the αth fragment molecule, the effective fragment potential $V_{\mathrm{el}}(\alpha, s)$ is given by

$$V_{\mathrm{el}}(\alpha,s)=\sum_{k=1}^{K} V_k^{\mathrm{elec}}(\alpha,s)+\sum_{l=1}^{L} V_l^{\mathrm{pol}}(\alpha,s)+\sum_{m=1}^{M} V_m^{\mathrm{rep}}(\alpha,s) \qquad (1)$$

where s denotes the electronic coordinates. The three terms on the right-hand side of Eq. (1) represent the aforesaid Coulombic, polarization, and exchange-repulsion/charge-transfer interactions. The Coulombic potential is expressed in terms of the distributed multipolar analysis (DMA) [30] of the charge distributions of the solvent. K in the first term of Eq. (1) is the total number of DMA expansion points. For instance, in the case of a H_2O molecule, those expansion points are the atom centers and the midpoints on the bonds. Each multipolar expansion is carried up to octupole terms at each expansion point. The entire expansion is multiplied by a distance-dependent cutoff function to account for overlapping charge densities. The polarization of the solvent induced by the electric field of the solute molecule is treated self-consistently [22,31]. In this procedure, the dipole polarizability tensor of the solvent molecules is expanded into its bond and lone-pair components of the localized orbital dipole polarizabilities that are placed at the centroids of the L localized valence molecular orbitals. The exchange-repulsion/charge-transfer interactions are modeled by simple Gaussian functions located at the fragment centers denoted by m in Eq. (1), where M is the total number of those centers. Again, in the case of a H_2O molecule, those expansion centers are each atom and the molecule center of mass. In the present EFP implementation, those Gaussian functions are fit to the residual energy in a series of water dimer conformations from which the electrostatic and polarization components have been subtracted [5,7,22,24]. Notwithstanding this fitting procedure, it is important to note that genuine charge transfers to or from the EFP region are not permitted in this method [5,7,22,24]. Finally, analogous terms are used to describe the fragment–fragment interactions. The EFP model as described herein is available in the electronic structure code GAMESS [32].

Geometry optimizations of the $LiOH(H_2O)_n$ ($n = 1–6, 8$) clusters were first calculated at the level of EFP/RHF theory with the quantum LiOH molecule described with the 6-311++G** basis set and the H_2O molecules by the EFP model (EFP/RHF/6-311++G**). To assess the accuracy of these EFP/RHF/6-311++G** calculations with respect to full ab initio methods, the EFP/RHF optimized geometries were used as the initial guesses for successive geometry optimizations at the RHF/6-311++G** and MP2/6-311++G** levels. The full RHF calculations will allow determining the degree of accuracy that might be lost by the Q/C procedure in the EFP/RHF method. It is important to bear in mind that the EFP method was designed to reproduce results at the Hartree–Fock level. MP2 calculations will allow determining the effect of electron correlation in this type of systems. Except for a few MP2 geometry optimizations involving analytical Hessian evaluations, all the present computational procedures were performed with the GAMESS program [32]. The MP2 analytical-Hessian calculations were performed with the GAUSSIAN 98 program [33].

3. Results and discussion

The calculated properties for the $LiOH(H_2O)_n$ ($n = 1–6, 8$) clusters are presented in Tables 1–8. Li–OH bond lengths, Li and O Mulliken charges, Li–OH bond orders and relative energies for each of the $LiOH(H_2O)_n$ ($n = 1–6, 8$) isomers at the EFP/RHF/6-311++G** level of theory are shown in Table 1. The same properties but at the RHF/6-311++G** and MP2/6-311++G** levels of theory are presented in Tables 2 and 3, respectively. Li–OH bond distances for the specific case of the $LiOH(H_2O)_6$ isomer **6za** with several basis sets and at the EFP/RHF/6-311++G**, RHF/6-311++G** and MP2/6-311++G** levels are listed in Table 4. Boltzmann-averaged values of the Li–OH bond lengths, Li and O Mulliken charges, and Li–OH bond orders for the $LiOH(H_2O)_n$ ($n = 1–6, 8$) clusters at the three levels of theory herein considered are listed in Tables 5–7. The differences in the Mulliken charges between the RHF/6-311++G** and the EFP/RHF/6-311++G** methods for each LiOH atom and for the whole LiOH molecule in the $LiOH(H_2O)_n$ ($n = 1–6, 8$) clusters are listed in Table 8. Finally, the structures of the $LiOH(H_2O)_n$ ($n = 1–6, 8$) clusters at the EFP/ RHF/6-311++G** level are depicted in Figs. 1–6, except for the case of the $LiOH(H_2O)_6$ isomer **6za** that is depicted at the RHF/6-311++G** level in Fig. 5. Some relevant bond lengths of the $LiOH(H_2O)_n$ ($n = 1–3$) clusters are also depicted in Figs. 1 and 2 along with their structures; however, the corresponding bond lengths of the remaining

Table 1
Structural and energetic properties for $LiOH(H_2O)_n$ ($n = 1–6,8$) with EFP/RHF/6-311++G**

Formula	Structure	R(Li–OH)	q(Li)	q(O)	BO	ΔE
$LiOH(H_2O)$	**1a**	1.619	0.650	−0.952	0.654	0.000
	1b	1.650	0.709	−1.002	0.551	0.175
$LiOH(H_2O)_2$	**2a**	1.676	0.752	−1.028	0.463	0.000
	2b	1.728	0.806	−1.094	0.366	2.615
$LiOH(H_2O)_3$	**3a**	1.841	0.888	−1.192	0.209	0.000
	3b	1.754	0.836	−1.110	0.306	−2.167
	3c	1.680	0.756	−1.023	0.456	0.150
$LiOH(H_2O)_4$	**4a**	1.776	0.856	−1.120	0.267	0.000
	4b	1.780	0.854	−1.119	0.270	0.505
	4c	1.809	0.882	−1.145	0.220	4.642
	4d	1.722	0.800	−1.056	0.373	5.969
	4e	1.787	0.871	−1.153	0.244	6.578
	4f	1.906	0.935	−1.240	0.119	7.775
$LiOH(H_2O)_5$	**5a**	1.781	0.865	−1.128	0.251	0.000
	5b	1.776	0.856	−1.121	0.266	1.930
	5c	1.859	0.924	−1.194	0.138	1.370
	5d	1.782	0.855	−1.120	0.268	2.183
	5f	1.784	0.868	−1.133	0.248	2.676
	5g	1.808	0.893	−1.167	0.199	0.790
	5h	1.828	0.908	−1.180	0.171	1.230
$LiOH(H_2O)_6$	**6a**	1.874	0.933	−1.201	0.123	0.000
	6b	1.861	0.926	−1.197	0.137	−0.286
	6c	1.853	0.909	−1.165	0.169	4.327
	6d	1.868	0.927	−1.181	0.135	1.201
	6f	1.871	0.932	−1.195	0.125	−0.231
	6i	1.777	0.853	−1.108	0.274	3.680
	6j	2.005	0.968	−1.263	0.000	3.807
	6l	1.900	0.947	−1.210	0.096	1.224
	6m	1.932	0.949	−1.238	0.085	2.913
	6n	1.858	0.916	−1.176	0.158	7.871
$LiOH(H_2O)_8$	**8a**	1.909	0.954	−1.213	0.083	0.000
	8b	1.879	0.937	−1.200	0.117	1.084
	8c	1.845	0.917	−1.178	0.154	1.961
	8d	1.870	0.927	−1.185	0.135	4.341
	8e	1.874	0.934	−1.195	0.122	1.809
	8f	1.872	0.926	−1.180	0.137	1.134
	8g	1.879	0.928	−1.183	0.133	2.383
	8h	1.872	0.926	−1.180	0.137	1.133
	8i	1.691	0.769	−1.038	0.431	16.665
	8j	1.735	0.816	−1.066	0.343	14.165
	8za	3.520	1.003	−1.255	0.000	4.249

Structure refers to the identification numbers in Figs. 1–6; R is the Li–OH bond length in Å, q(Li) is the Mulliken charge on Li, q(O) is the Mulliken charge on O, BO is the Li–OH bond order, and ΔE is the energy relative to the isomer **a** in kcal/mol.

Table 2
Structural and energetic properties for $LiOH(H_2O)_n$ ($n = 1–6,8$) with RHF/6-311++G**

Formula	Structure	R(Li–OH)	q(Li)	q(O)	BO	ΔE
$LiOH(H_2O)$	**1a**	1.616	0.519	−0.887	0.762	0.000
	1b	1.668	0.597	−0.972	0.588	−1.440
$LiOH(H_2O)_2$	**2a**	1.685	0.618	−0.976	0.538	0.000
	2b	1.759	0.455	−0.970	0.464	0.839
$LiOH(H_2O)_3$	**3a**	1.868	0.286	−1.003	0.436	0.000
	3b	1.780	0.561	−0.983	0.405	−1.637
	3c	1.689	0.604	−0.958	0.535	1.381
$LiOH(H_2O)_4$	**4a**	1.796	0.616	−0.969	0.400	0.000
	4b	1.800	0.629	−0.964	0.381	0.079
	4c	1.832	0.471	−0.944	0.477	4.233
	4d	1.729	0.577	−0.951	0.524	6.555
	4e	1.785	0.580	−0.973	0.409	3.632
	4f	1.905	0.223	−1.041	0.410	9.538
$LiOH(H_2O)_5$	**5a**	1.787	0.500	−0.969	0.502	0.000
	5b	1.787	0.559	−0.960	0.430	1.125
	5c	1.869	0.514	−0.980	0.423	0.225
	5d	1.787	0.556	−0.959	0.432	1.128
	5f	1.798	0.475	−0.937	0.515	1.730
	5g	1.813	0.520	−1.036	0.405	0.415
	5h	1.844	0.431	−1.021	0.408	1.595
$LiOH(H_2O)_6$	**6a**	1.884	0.579	−1.055	0.353	0.000
	6b	1.880	0.529	−0.989	0.417	−0.679
	6c	1.850	0.505	−0.938	0.429	3.382
	6d	1.866	0.580	−1.003	0.375	−0.896
	6f	1.883	0.553	−1.052	0.367	−0.057
	6i	1.799	0.583	−0.937	0.414	1.571
	6j	1.979	0.418	−1.120	0.169	5.698
	6l	1.882	0.532	−1.019	0.426	−0.516
	6m	1.883	0.546	−1.047	0.367	−0.057
	6n	1.789	0.509	−0.952	0.448	1.012
	6za	3.689	0.356	−1.073	0.000	2.761
$LiOH(H_2O)_8$	**8a**	1.907	0.553	−1.082	0.315	0.000
	8f	1.885	0.528	−0.966	0.398	1.721
	8za	3.383	0.449	−1.086	0.100	7.469

Structure refers to the identification numbers in Figs. 1–6; R is the Li–OH bond length in Å, q(Li) is the Mulliken charge on Li, q(O) is the Mulliken charge on O, BO is the Li–OH bond order and ΔE is the energy relative to the isomer **a** in kcal/mol.

$LiOH(H_2O)_n$ ($n = 5, 6, 8$) clusters are omitted in their figures for the sake of clarity.

3.1. Equilibrium geometries, relative energies and dissociation processes

The Li–OH bond distance in the gas phase is predicted to be 1.590 and 1.607 Å at the RHF/6-311++G** and MP2/6-311++G** levels of theory, respectively. These values will be taken as the theoretically exact Li–OH bond lengths of the LiOH molecule to scrutinize the onset of the LiOH dissociation. When for a given $LiOH(H_2O)_n$ ($n = 1–6, 8$) isomer, the Li–OH bond length is equal to or longer than twice the value of those theoretical bond lengths (i.e. 3.180 and 3.214 Å, respectively), the LiOH molecule within the cluster will be considered as dissociated into a Li^+/OH^- separated ion pair. Otherwise, the LiOH molecule will be considered as non-dissociated and therefore classified as a contact ion pair. Except for one intermediate case in one of the $LiOH(H_2O)_3$ isomers at the MP2/6-311++G** level, all the calculated LiOH molecules within the clusters can be categorized into either a dissociated Li^+/OH^- separated ion pair or a non-dissociated contact ion pair.

3.1.1. $LiOH(H_2O)$

In the case of the $LiOH(H_2O)$ clusters, two stable isomers, where found, whose structures at the EFP/RHF/6-311++G** level are depicted in Fig. 1. Examination of the calculated optimal geometries reveals

Table 3
Structural and energetic properties for $LiOH(H_2O)_n$ ($n = 1$–6,8) with MP2/6-311++G**

Formula	Structure	R(Li–OH)	q(Li)	q(O)	BO	ΔE
$LiOH(H_2O)$	**1a**	1.629	0.534	−0.864	0.760	0.000
	1b	1.702	0.596	−0.933	0.550	−3.401
$LiOH(H_2O)_2$	**2a**	1.721	0.638	−0.945	0.486	0.000
	2b	1.836	0.494	−0.947	0.361	1.027
$LiOH(H_2O)_3$	**3a**	2.558	0.535	−1.014	0.000	0.000
	3b	1.840	0.564	−0.954	0.341	0.006
	3c	1.728	0.634	−0.930	0.469	3.525
$LiOH(H_2O)_4$	**4a**	1.848	0.657	−0.963	0.324	0.000
	4b	1.850	0.669	−0.965	0.305	0.180
	4c	1.892	0.494	−0.922	0.359	3.921
	4d	1.767	0.647	−0.921	0.435	7.049
	4e	1.912	0.579	−0.938	0.255	5.234
	4f	2.073	0.299	−1.017	0.233	8.952
$LiOH(H_2O)_5$	**5a**	1.833	0.550	−0.957	0.394	0.000
	5b	1.831	0.577	−0.946	0.356	1.222
	5c	1.956	0.540	−0.961	0.303	−0.340
	5d	1.837	0.606	−0.949	0.339	1.291
	5f	1.862	0.518	−0.921	0.394	1.535
	5g	1.857	0.555	−1.044	0.325	0.242
	5h	1.892	0.444	−1.014	0.329	0.644
$LiOH(H_2O)_6$	**6a**	1.937	0.567	−1.043	0.284	0.000
	6b	1.927	0.618	−1.010	0.276	−0.366
	6c	1.904	0.667	−0.992	0.294	4.949
	6d	1.930	0.641	−0.981	0.252	−1.265
	6f	1.932	0.609	−1.088	0.247	0.121
	6i	1.842	0.630	−0.942	0.350	3.320
	6j	1.980	0.416	−1.055	0.292	0.607
	6l	1.941	0.650	−1.041	0.276	0.426
	6m	2.003	0.495	−1.011	0.138	2.262
	6n	1.977	0.544	−0.991	0.257	6.766
	6za	3.721	0.384	−0.965	0.000	−1.769
$LiOH(H_2O)_8$	**8a**	1.956	0.627	−1.098	0.178	0.000
	8f	1.931	0.612	−0.981	0.280	1.580
	8za	3.422	0.528	−1.036	0.070	4.308

Structure refers to the identification numbers in Figs. 1–6; R is the Li–OH bond length in Å, q(Li) is the Mulliken charge on Li, q(O) is the Mulliken charge on O, BO is the Li–OH bond order and ΔE is the energy relative to the isomer **a** in kcal/mol.

that in isomer **1a**, the O–Li–O bond angle is of 158° at the EFP/RHF/6-311++G** level, while it is of 180° at the RHF/6-311++G** and MP2/6-311++G** ones (C_2 symmetry). Contrastingly, in the case of the $NaOH(H_2O)$ clusters, an isomer analogous to **1a** presents a C_2 symmetry at the three levels of theory herein considered [5]. On the other hand, the geometries and shapes of the $LiOH(H_2O)$ isomer **1b** remain similar at the three levels of theory. In addition, the Li–O–H bond angle at the EFP/RHF/6-311++G** level measures 178 and 163° in isomers **1a** and **1b**, respectively, being the LiOH molecule almost linear in the first isomer. Isomer **1b** turns out to be more stable than **1a** at the RHF6-311++G** and the MP2/6-311++G** levels, but a reverse order of stability shows at the EFP/RHF/6-311++G** one. No dissociation of LiOH into a Li^+/OH^- separated ion pair is observed in this series of clusters.

Table 4
Li–OH bond length for the C_3-symmetry $Li(OH)(H_2O)_6$ isomer **6za** at the EFP, RHF, and MP2 levels of theory with several basis sets

Basis set	EFP/RHF R(Li–OH)	RHF R(Li–OH)	MP2 R(Li–OH)
6-31G	3.483	3.841	3.836
6-31G**	No convergence	Not performed	Not performed
6-31++G	3.824	3.855	3.852
6-31++G**	No convergence	Not performed	Not performed
6-311G	3.574	3.828	3.814
6-311G**	3.223	3.672	3.659
6-311++G	3.827	3.862	3.829
6-311++G**	No convergence	3.689	3.721
6-311++G (3df, 3pd)	3.776	3.567	3.629
6-311++G (2d, 2p)	1.948	3.544	No convergence
6-311G (2df, 2pd)	1.848	3.554	No convergence
cc-pVDZ	No convergence	Not performed	Not performed
cc-PVTZ	3.489	Not performed	Not performed
STO-3G	No convergence	Not performed	Not performed

R is the Li–OH bond length in Å at the indicated methods.

3.1.2. $LiOH(H_2O)_2$

In the case of the $LiOH(H_2O)_2$ clusters, two stable isomers were found whose structures at the EFP/RHF/6-311++G** level are depicted in Fig. 1. Isomer **2a** exhibits a ring structure involving the three molecules of the cluster: the LiOH and the two H_2O molecules. One of the H_2O molecules is directly bonded to the LiOH, whereas the second H_2O molecule is hydrogen-bonded to both the first H_2O molecule and the OH group of LiOH through its O and through one of its H atoms, respectively. Isomer **2b** presents two strained rings, where the two O atoms of the H_2O molecules are directly bonded to the Li atom, whereas one H atom per each H_2O molecule is hydrogen-bonded to the OH group of LiOH. Both isomers **2a** and **2b** present bent LiOH molecules with Li–O–H bond angles measuring 152 and 159°, respectively, at the EFP/RHF/6-311++G** level of theory. The relative energy of isomer **2b** is higher than that

Table 5
Boltzmann-averaged values of relevant structural properties for $LiOH(H_2O)_n$ ($n = 1$–6,8) with EFP/RHF/6-311++G**

n	$\langle R$(Li–OH)$\rangle$	$\langle q$(Li)$\rangle$	$\langle q$(O)$\rangle$	$\langle$BO$\rangle$
0	1.590	0.614	−0.928	0.734
1	1.633	0.677	−0.975	0.607
2	1.679	0.756	−1.033	0.457
3	1.756	0.834	−1.110	0.309
4	1.778	0.855	−1.120	0.268
5	1.800	0.881	−1.149	0.220
6	1.871	0.931	−1.197	0.127
8	1.897	0.940	−1.198	0.110

Boltzmann-averaged structural properties at $T = 298$ K calculated with the zero-point E_0 energies within the harmonic approximation. R is the Li–OH bond length in Å, q(Li) is the Mulliken charge on Li, q(O) is the Mulliken charge on O, and BO is Li–OH bond order.

Table 6
Boltzmann-averaged values of relevant structural properties for $LiOH(H_2O)_n$ ($n = 1$–6,8) with RHF/6-311++G**

n	$\langle R(\text{Li–OH})\rangle$	$\langle q(\text{Li})\rangle$	$\langle q(\text{O})\rangle$	$\langle \text{BO}\rangle$
0	1.590	0.614	−0.928	0.734
1	1.658	0.583	−0.956	0.621
2	1.707	0.570	−0.974	0.516
3	1.790	0.520	−0.985	0.415
4	1.798	0.620	−0.967	0.392
5	1.815	0.512	−0.984	0.448
6	1.873	0.552	−1.015	0.392

Boltzmann-averaged values at $T = 298$ K calculated with the zero-point E_0 energies within the harmonic approximation. R is the Li–OH bond length in Å, q(Li) is the Mulliken charge on Li, q(O) is the Mulliken charge on O, and BO is Li–OH bond order.

of **2a** by 2.615, 0.839 and 1.027 kcal/mol at EFP/RHF/6-311++G**, RHF/6-311++G**, and MP2/6-311++G** levels of theory, respectively. The Li–OH bond lengths for isomer **2a** measure: 1.676, 1.685, and 1.721 Å, at the aforesaid three levels of theory, respectively, values that are shorter than its isomer **2b** counterparts of: 1.728, 1.759, 1.836 Å, respectively. No dissociation of LiOH into a Li^+/OH^- separated ion pair is observed in this series of clusters.

3.1.3. $LiOH(H_2O)_3$

In the case of the $LiOH(H_2O)_3$ clusters, three stable isomers were found whose structures at the EFP/RHF/6-311++G** level are depicted in Fig. 2. Isomer **3a** has a C_3 symmetry with the C_3 rotational axis along the aligned Li–O–H atoms. In this isomer, the Li–OH bond length measures 2.558 Å at the MP2/6-311++G** level of theory, a value that is somewhat longer than its counterparts of 1.841 and 1.868 Å at the EFP/RHF/6-311++G** and RHF/6-311++G** levels, respectively. Therefore, in a MP2/6-311++G** calculation, the LiOH molecule in the $LiOH(H_2O)_3$ isomer **3a** has an intermediate character between contact and separated ion pairs. In the case of isomers **3b** and **3c**, large differences in the Li–OH bond lengths are not observed at **3b** any of the three levels of theory herein considered. Unlike the C3-symmetry isomer **3a**, isomers **3b** and **3c** do display ring structures where hydrogen bonding plays a prominent role. Isomer **3b** exhibits two strained rings involving one and two H_2O molecules, respectively, and has the LiOH molecule acting as the linkage between both rings. Isomer **3c** exhibits a single less-strained ring involving the four molecules in the cluster. The LiOH molecule is linear in isomer **3a** but bent in the other two isomers. The energy of the isomer **3b** turns out to be the lowest of the three $LiOH(H_2O)_3$ structures at the EFP/RHF6-311++G** and the RHF/6-311++G** levels, whereas both isomers **3a** and **3b** are much more stable than isomer **3c** at the MP2/6-311++G** level.

Table 7
Boltzmann-averaged values of relevant structural properties for $LiOH(H_2O)_n$ ($n = 1$–6,8) with MP2/6-311++G**

n	$\langle R(\text{Li–OH})\rangle$	$\langle q(\text{Li})\rangle$	$\langle q(\text{O})\rangle$	$\langle \text{BO}\rangle$
0	1.607	0.593	−0.889	0.745
1	1.700	0.594	−0.931	0.556
2	1.751	0.601	−0.946	0.453
3	2.194	0.551	−0.984	0.174
4	1.849	0.660	−0.963	0.316
5	1.884	0.539	−0.977	0.340
6	2.688	0.514	−0.994	0.152

Boltzmann-averaged values at $T = 298$ K calculated with the zero-point E_0 energies within the harmonic approximation. R is the Li–OH bond length in Å, q(Li) is the Mulliken charge on Li, q(O) is the Mulliken charge on O, and BO is Li–OH bond order.

Table 8
Differences in the Mulliken charges between RHF/6-311++G**and EFP/RHF/6-311++G** for each LiOH atom and for the whole LiOH molecule in several $LiOH(H_2O)_n$ ($n = 1$–6,8) clusters

Formula	Structure	Δq_{Li}	Δq_{O}	Δq_{H}	Δq_{LiOH}
$LiOH(H_2O)$	**1a**	−0.131	0.065	−0.004	−0.070
	1b	−0.112	0.030	0.010	−0.072
$LiOH(H_2O)_2$	**2a**	−0.134	0.052	0.021	−0.061
	2b	−0.351	0.124	−0.004	−0.231
$LiOH(H_2O)_3$	**3a**	−0.602	0.189	0.020	−0.393
	3b	−0.275	0.127	−0.007	−0.155
	3c	−0.152	0.065	0.017	−0.070
$LiOH(H_2O)_4$	**4a**	−0.240	0.151	−0.013	−0.102
	4b	−0.225	0.155	−0.021	−0.091
	4c	−0.411	0.201	−0.007	−0.217
	4d	−0.223	0.105	0.025	−0.093
	4e	−0.291	0.180	−0.026	−0.137
$LiOH(H_2O)_5$	**5a**	−0.365	0.159	0.032	−0.174
	5b	−0.297	0.161	0.000	−0.136
	5c	−0.410	0.214	0.004	−0.192
	5d	−0.299	0.161	0.000	−0.138
	5f	−0.393	0.196	0.030	−0.167
	5g	−0.373	0.131	0.032	−0.210
	5h	−0.477	0.159	0.038	−0.280
$LiOH(H_2O)_6$	**6a**	−0.354	0.146	0.029	−0.179
	6b	−0.397	0.208	0.016	−0.173
	6c	−0.404	0.227	−0.011	−0.188
	6d	−0.347	0.178	0.010	−0.159
	6f	−0.379	0.143	0.042	−0.194
	6i	−0.270	0.171	−0.013	−0.112
	6j	−0.550	0.143	0.023	−0.384
	6l	−0.415	0.191	0.027	−0.197
	6m	−0.403	0.191	0.015	−0.197
	6n	−0.407	0.224	0.023	−0.160
	6za	–	–	–	−0.441
$LiOH(H_2O)_8$	**8a**	−0.401	0.131	0.051	−0.219
	8f	−0.398	0.214	0.011	−0.173
	8za	−0.554	0.169	0.008	−0.377

Structure refers to the identification numbers in Figs. 1–6; each difference in the Mulliken charges Δq_X(X = Li, O, H, LiOH) is defined as $\Delta q_X = q_X^{\text{RHF}} - q_X^{\text{EFP}}$, i.e. as the excess (+) or defect (−) of charge in RHF with respect to EFP. Δq_{LiOH} expresses the total charge on the LiOH solute in RHF because $q_{\text{LiOH}}^{\text{EFP}} = 0$.

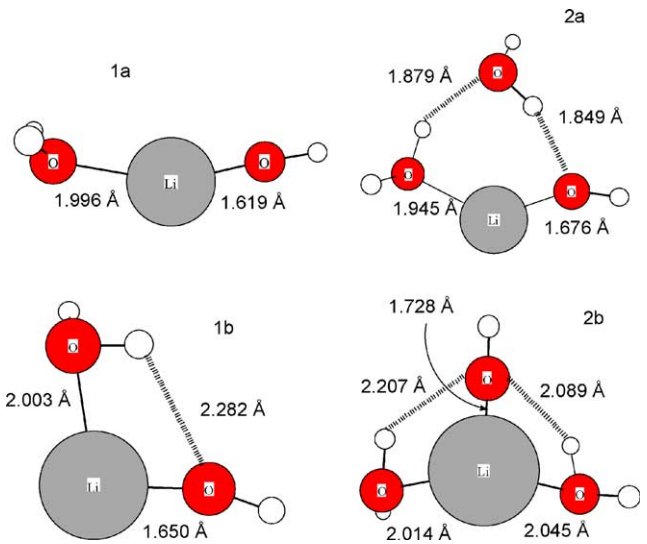

Fig. 1. Structures of the $LiOH(H_2O)$ and $LiOH(H_2O)_2$ isomers at the EFP/RHF/6-311++G** level.

3.1.4. $LiOH(H_2O)_4$

In the case of the $LiOH(H_2O)_4$ clusters, six stable structures were found whose structures at the EFP/RHF/6-311++G** level are depicted in Fig. 3. Except for isomer **4f**, all the calculated clusters display ring structures, where again hydrogen bonding plays a prominent role. Both isomers **4a** and **4b** exhibit pairs of similar rings, each ring having two H_2O molecules, and have the LiOH molecule acting as the linkage between both rings. Isomer

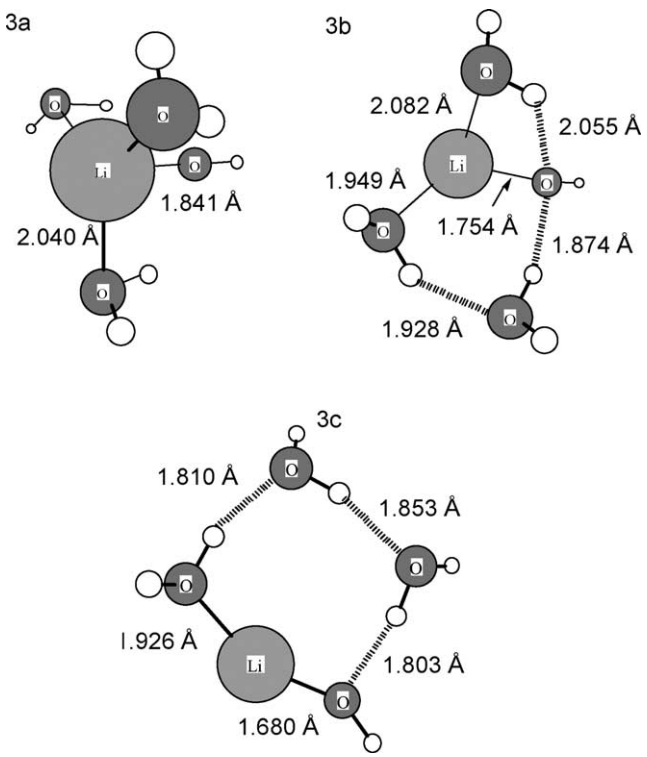

Fig. 2. Structures of the $LiOH(H_2O)_3$ isomers at the EFP/RHF/6-311++G** level.

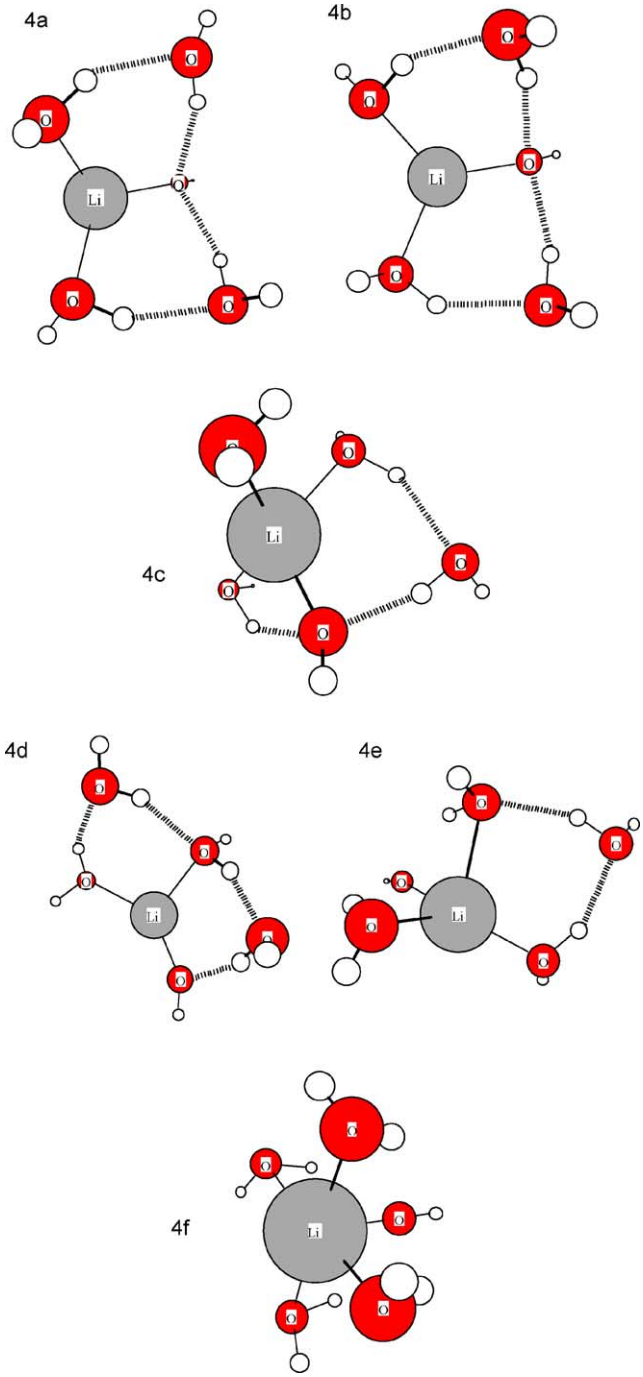

Fig. 3. Structures of the $LiOH(H_2O)_4$ isomers at the EFP/RHF/6-311++G** level.

4d displays two different rings involving two and three H_2O molecules, respectively, and has the $Li-H_2O$ acting as the linkage between the two rings. Both isomers **4c** and **4e** have one ring involving three of the four H_2O molecules. Isomer **4f** has a C_4 symmetry, being therefore the only structure for the $LiOH(H_2O)_4$ clusters not exhibiting rings. In the previously considered C_3-symmetry $LiOH(H_2O)_3$ isomer **3a**, the Li–OH bond distance turned out to be much longer at the MP2/6-311++G** level than at the two others.

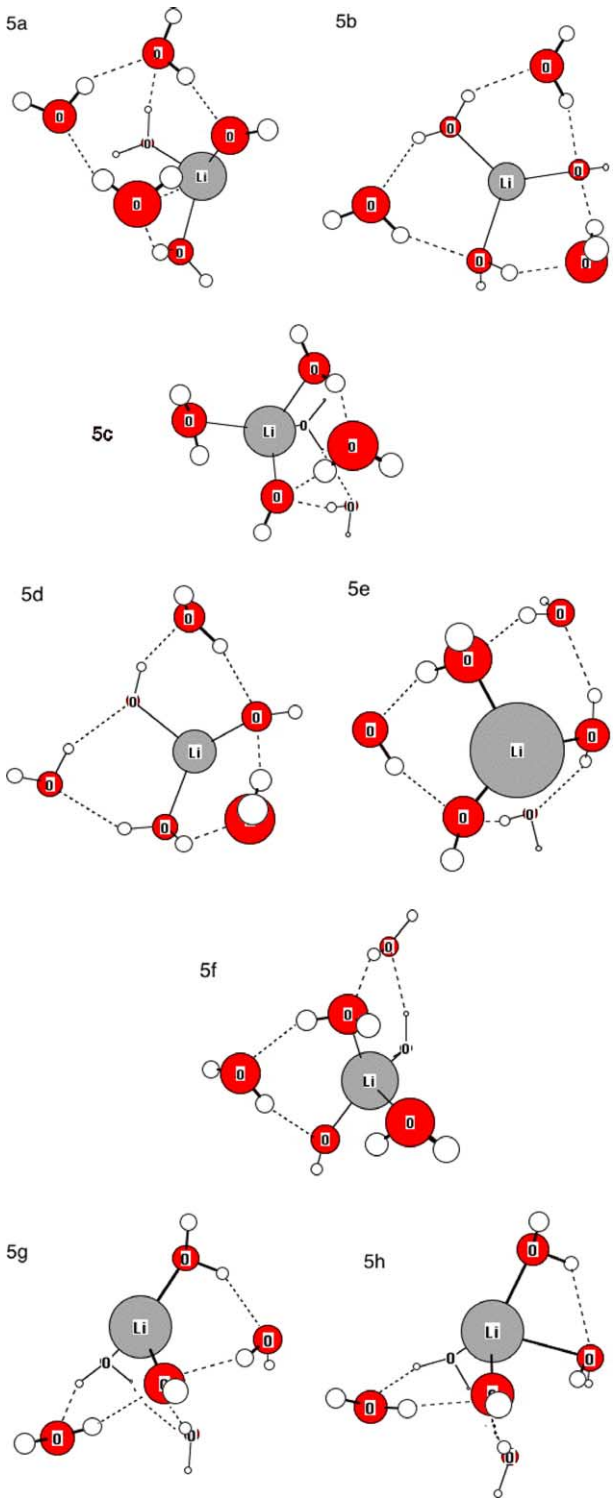

Fig. 4. Structures of the $LiOH(H_2O)_5$ isomers at the EFP/RHF/6-311++G** level.

However, this situation is not observed in the C_4-symmetry $LiOH(H_2O)_4$ isomer **4f**, where the Li–OH bond length is somewhat longer in a MP2/6-311++G** calculation but not longer enough to classify this structure as an intermediate case between contact and separated ion pairs. Overall, isomer **4f** has the longest Li–OH bond distance in the $LiOH(H_2O)_4$ series of isomers at the three levels of theory herein considered. In addition, isomer **4a** and **4b** have the lowest energies under the three methods of calculation. No dissociation of LiOH into a Li^+/OH^- separated ion pair is observed in this series of clusters.

3.1.5. $LiOH(H_2O)_5$

In the case of the $LiOH(H_2O)_5$ clusters, eight stable isomers were found whose structures at the EFP/RHF/6-311++G** level are depicted in Fig. 4. For the specific case of the MP2/6-311++G** method, previously shown calculation for the $LiOH(H_2O)_n$ ($n = 1$–4) clusters via numerical evaluation of the MP2 Hessian have always rendered stable structures with all their normal-mode frequencies real. However, this type of calculations for the $LiOH(H_2O)_5$ clusters rendered at times some unstable structures with a few imaginary frequencies as a result of the limited accuracy of the numerical MP2 Hessian algorithm. Therefore, more accurate MP2/6-311++G** calculations involving analytical MP2 Hessian evaluations were performed by which structures with all their normal-mode frequencies real were finally obtained. All the stable $LiOH(H_2O)_5$ isomers exhibit ring structures, where hydrogen bonding again plays a prominent role. Isomers **5a**, **5b**, **5d**, **5e** and **5g** display three rings, whereas isomers **5c**, **5f** and **5h** display only two. Isomer **5a** is the most stable structure at the first two levels of theory herein considered and exhibits three rings: one involving three H_2O molecules and the other two involving two H_2O molecules each. Isomer **5b** has a relatively flat structure and exhibits three rings: one involving three H_2O molecules and the other two involving two H_2O molecules each; the LiOH molecule acts as the linkage between two of the three rings. On the other hand, isomers **5c** and **5f** exhibit two rings involving varying numbers of H_2O molecules each and both isomers have an extra H_2O molecule, not involved in the rings, directly bonded to the Li atom through its O atom. Similar ring structures can be discerned in the remaining isomers as shown in Fig. 4. In the $LiOH(H_2O)_5$ series of isomers, the calculated relative energies and Li–OH bond lengths slightly vary at each of the three levels of theory, with a deviation of about 2 kcal/mol in the case of the relative energies. No dissociation of LiOH into a Li^+/OH^- separated ion pair is observed in this series of clusters.

3.1.6. $LiOH(H_2O)_6$

In the case of the $LiOH(H_2O)_6$ clusters, eleven stable isomers were found whose structures are depicted in Fig. 5 at the EFP/RHF/6-311++G** level, except for isomer **6za** whose EFP/RHF/6-311++G** calculation failed to converged and is therefore depicted at the RHF/6-311++G** level. Isomer **6za** stands out amongst these structures because of its clear exhibition of LiOH dissociation and of its seemingly cubic symmetry. No LiOH dissociation is observed in any of the other ten $LiOH(H_2O)_6$ isomers. Isomer **6za** has a net C_3 symmetry with its C_3 axis along

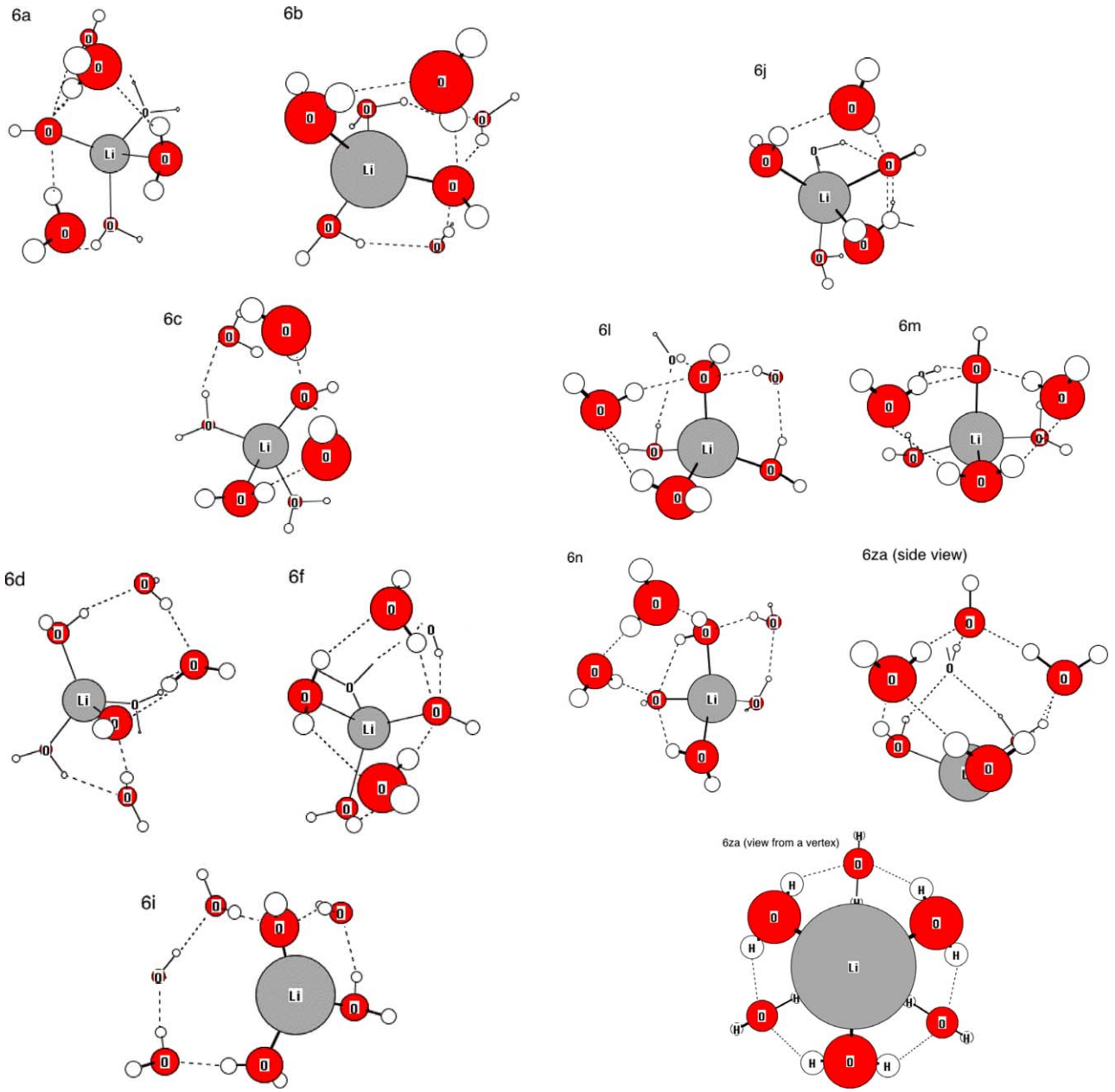

Fig. 5. Structures of the $LiOH(H_2O)_6$ isomers at the EFP/RHF/6-311++G** level (Isomer **6za** is the only one shown at the RHF/6-311++G** level).

the aligned Li–O–H atoms and with the coordinated H_2O molecules arranged in accordance with the overall symmetry. Moreover, the Li and the O atoms of the original LiOH molecule and the six O atoms of the six H_2O molecules are placed on the eight vertices of a distorted cube with the C_3 Li–O–H axis coinciding with one of the C_3 axis of the cube. The distorted shape of the cube and the H atoms additionally bonded to the O atoms on the cube vertices prevent isomer **6za** from adopting a perfect O_h symmetry. Inspection of the data in Tables 2 and 3 reveals that the Li–OH bond length in isomer **6za** measures 3.689 and 3.721 Å at the RHF/6-311++G** and MP2/6-311++G** levels, respectively, thereby revealing the LiOH dissociation into a Li^+/OH^- separated ion pair. In addition, that predicted separated ion pair turns out to be the most stable structure in the $LiOH(H_2O)_6$ series of isomers at the MP2/6-311++G** level of theory. Unfortunately, the corresponding EFP/RHF/6-311++G** calculation for isomer **6za** failed to converge and the expected dissociation prediction by this method could not be made. Therefore, a complete series of calculations for the C_3-symmetry $LiOH(H_2O)_6$ isomer **6az** were performed with several basis sets in order to confirm the LiOH dissociation at the three levels of theory. The Li–OH bond lengths from those calculations are listed in Table 4. The results from all those available calculations at the RHF and MP2 levels support without exception the predicted LiOH dissociation in isomer **6az**. With several basis sets: 6-31G, 6-31++G,

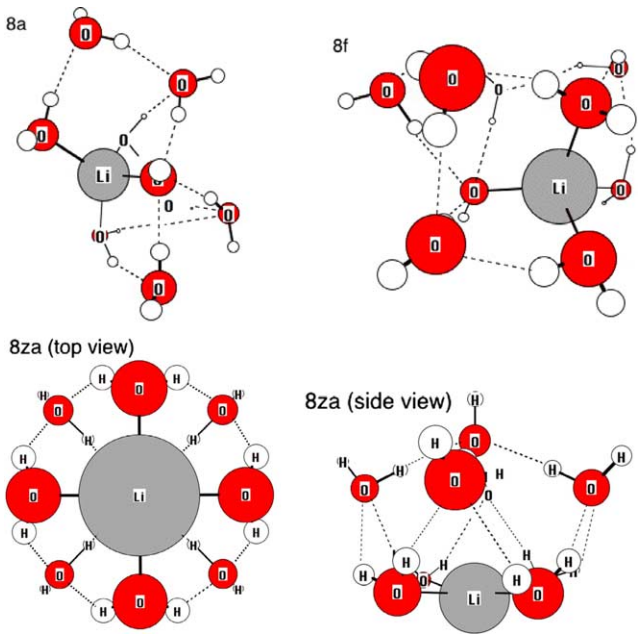

Fig. 6. Structures of the $LiOH(H_2O)_8$ isomers at the EFP/RHF/6-311++G** level.

6-311G, 6-311G**, 6-311++G, 6-311++G(3df, 3pd) and cc-pVTZ, the EFP/RHF calculations do converge with their resulting values for the Li–OH bond lengths consistent with a LiOH dissociation and in satisfactory agreement with the available quantum mechanics results. In contrast, the EFP/RHF calculations with the 6-311++G(2d, 2p) and 6-311++G(2df, 2pd) basis sets converge but do not predict LiOH dissociation and no convergence is achieved with the few remaining basis sets herein tested.. The data listed in Table 4 suggest that diffusion functions slightly increases the Li–OH bond distances, whereas polarization functions shorten them. When dissociation is predicted by EFP/RHF calculations, the Mulliken charge on the Li atom always remains close to 1.0 (Li^{+1}) whereas that on the O atom ranges from −1.4 to −1.2. On the contrary, in the non-dissociating EFP/RHF/6-311G(2df, 2pd) calculation, the Mulliken charges on the Li and the O atoms are 0.66 and −0.85, respectively. This indicates that the Mulliken charge on the Li atom in an EFP/RHF calculation is close to 1.0 at dissociation but becomes fractional and lower than 1.0 when dissociation is not predicted. The situation is not so sharply defined for the full quantum mechanics calculations, which always predict dissociation, because the Mulliken charge on the Li atom is 0.36 and 0.38 at the RHF/6-311++G** and MP2/6-311++G** levels but it is about 1.0 at both the RHF/6-311(3df, 3pd) and MP2/6-311 ones.

Isomers **6a**–**6n** are rather asymmetrical structures in comparison with the previously discussed isomer **6za** and display no instance of LiOH dissociation. Those structures exhibit an astonishing wealth of shapes that defies any detailed written description. The number of ring structures per isomer ranges from two to five, and some rings are interconnected. Isomer **6a** exhibits three rings involving two H_2O molecules each and with the LiOH molecule acting as a linkage of the three rings. Isomers **6c** and **6j** are structurally the simplest in this series, having only two rings each. In isomer **6c**, one ring involves two H_2O molecules, whereas the other involves three; an extra H_2O molecule, not involved in the rings, is directly bonded to the Li atom. The structures of other $LiOH(H_2O)_6$ isomers can be discerned in Fig. 5. It is worth noticing that the geometry of isomer **6m** is a distorted form of the C_3-symmetry **6za** isomer structure. At each of the three levels of theory herein considered, the values of the Li–OH bond lengths slightly varies over the non-dissociating series of $LiOH(H_2O)_6$ isomers **6a**–**6n**. However, the relative energies exhibit a somewhat large deviation of about 8 kcal/mol over the complete series of $LiOH(H_2O)_6$ isomers.

3.1.7. $LiOH(H_2O)_8$

In the case of the $LiOH(H_2O)_8$ clusters, eleven stable isomers were found at the EFP/RHF/6-311++G** level but only three of them, isomers **8a**, **8f** and **8za** could be calculated at the RHF/6-311++G** and MP2/6-311++G** levels at the time of this report; the structures of these three isomers are depicted in Fig. 6 at the EFP/RHF/6-311++G** level. Isomer **8az** stands out amongst these structures because of its clear exhibition of LiOH dissociation at the three levels of theory and of its highly symmetric structure. Isomer **8za** has a net C_4 symmetry with its C_4 axis along the aligned Li–O–H atoms; this axis is encircled by two crowns of four H_2O molecules each whose O atoms are arranged in a D_{4d} symmetry. The internuclear lines along each pair of H atoms in the four H_2O molecules of the upper crown are directed toward the C_4 axis in an approximately radial direction, whereas those internuclear lines in the lower crown are tangential. Contrastingly, isomers **8a** and **8f** do not exhibit LiOH dissociation, have no definite symmetry, and display several ring structures. In these three isomers, the stability decreases in the order: **8a**, **8f** and **8za** at the three levels of theory herein considered.

3.2. Boltzmann averages and comparison with previous theoretical work

In order to determine on a quantitative basis the clusters dissociation trends and to acquire a picture of the solute situation in a bulk solution, Boltzmann distribution averages at the absolute temperature $T = 298$ K for the Li–OH bond lengths, Li Mulliken charges, O Mulliken charges, and Li–OH bond orders were calculated at the three levels of theory herein considered for each of the $LiOH(H_2O)_n$ ($n = 1–6, 8$) series of isomers. These calculations were based on the zero-point, relative energies of the isomers within the harmonic approximation. The results of this averaging procedure are listed in Tables 5–7 at the EFP/RHF/6-311++G**, RHF/6-311++G** and MP2/6-311++G** levels of theory, respectively. In the first

two methods, the Boltzmann-averaged Li–OH bond length (bond order) monotonically increases (almost monotonically decreases) as the number of H_2O molecules increases from 0 to 8. In the case of the MP2/6-311++G** calculations, the same trend is observed but with a sudden peak (dip) in the averaged Li–OH bond length (bond order) at the $LiOH(H_2O)_3$ clusters as a result of the predominant contribution to the average by the most stable and partially dissociated $LiOH(H_2O)_3$ isomer **3a**. The observed trends in the averaged Li–OH bond lengths and orders clearly indicate the propensity of the LiOH solute molecule to dissociate into a Li^+/OH^- separated ion pair as the number of solvent molecules increases.

An important aspect in the present investigation is to determine the correctness of the atomic charge description on the LiOH solute by EFP and the related effect of genuine charge transfer from or to the solvent on the accuracy of the EFP calculations. As mentioned before, genuine charge transfers to or from the EFP region are not permitted in this method. To account for charge-transfer effects, the EFP charge-transfer component of the energy was originally fitted to a series of H_2O dimers [22]. Since charge transfer does not play a prominent role in those pure H_2O systems, the accuracy of EFP when applied to ionic systems like the $LiOH(H_2O)_n$ ($n = 1–6, 8$) clusters, where charge transfer is expected to be relevant, should be scrutinized. Merrill, Webb and co-workers have carefully investigated these charge-transfer issues in EFP during their detailed studies on aqueous alkali metal-, alkaline-earth metal- and (oxy)anion-water ions [24,26,27]. By comparing EFP, RHF and MP2 results, these authors could determine that at the ab initio level of description, charge transfers from or to the solvent were substantial in the smallest-size ions therein studied: $Li^+(H_2O)_{1-6}$, $Mg^{+2}(H_2O)_{1-6}$, and $OH^-(H_2O)_{1-6}$, but far less extensive in their related largest-size ions: $Na^+(H_2O)_{1-6}$ and $K^+(H_2O)_{1-6}$; $Ca^{2+}(H_2O)_{1-6}$; and $Br^-(H_2O)_{1-6}$, respectively. In the case of the $Mg^{+2}(H_2O)_{1-6}$ ions [24], the large extent of electron transfer from the solvent and the impossibility of EFP to explicitly describe it have caused this method to inaccurately reproduce the RHF enthalpies of hydration and to predict incorrectly longer $Mg^{+2}\cdots O$ bonds. In the case of the $OH^-(H_2O)_{1-6}$ ions [26], the large extent of charge transfer has prevented EFP for consistently reproducing the RHF results and even this method was inadequate to model the mono-hydrated ion $OH(H_2O)_1$. Quite remarkably, the extent of charge transfer was also considerable in the $Li^+(H_2O)_{1-6}$ ions [24] (for instance, 0.32 e^- have been transferred to the Li^+ in the $Li^+(H_2O)_6$ ion) but the agreement between EFP and RHF in both structural and energetic properties was excellent. The authors then concluded that EFP can accurately reproduce the effect of an electron transfer of up to 0.13 e^- per H_2O molecule in the $Li^+(H_2O)_{1-6}$ series of ions.

For the present case of the $LiOH(H_2O)_n$ ($n = 1–6, 8$) clusters, inspection of Tables 1–3 reveals that the Mulliken charges on the Li and O atoms of the LiOH solute at the EFP/RHF/6-311++G** level do not agree well with those at the RHF/6-311++G** level, whereas those charge values at the RHF/6-311++G** and MP2/6-311++G** levels agree reasonably between themselves. The charge disagreement between EFP/RHF/6-311++G** and RHF/6-311++G** is more severe in the Mulliken charges on the Li atom than in those on the O atom. The EFP/RHF/6-311++G** method consistently predicts more positive Mulliken charges on the Li atom than its ab initio counterparts. Far more importantly, the Mulliken charge on the Li atom sharply increases as more H_2O molecules are added to the solute at the EFP/RHF/6-311++G** level but varies slightly at the two other levels of theory. The limiting value of the Li Mulliken charge with eight H_2O molecules is in most of the cases within the range of + 0.9 to + 1.0 (Li^{+1}) at the EFP/RHF/6-311++G** level but mostly within the range of + 0.4 to + 0.6 at the other two levels. These divergent charge trends between the EFP and the ab initio methods also manifest in the Boltzmann-averaged Mulliken charges shown in Tables 5–7. Therefore, EFP predicts that LiOH will tend to form contact or separated ion pairs having net Li^{+1} and OH^- ions with almost integer Mulliken charges +1 and −1, respectively, as the number of solvent molecules increases. This effect seems to be caused by the EFP field on LiOH by somehow favoring an internal redistribution of the solute charges into Li^{+1} and OH^- ions as successive H_2O molecules are added. However, comparison with ab initio results shows that such EFP solute charge separation is not genuine because the Mulliken charges on the Li and O atoms do not vary appreciably with the number of H_2O molecules in RHF and MP2 and, roughly speaking, remain around the values + 0.5 and − 1.0, respectively. If one assumes that the Coulombic and polarization fields by the EFP and the ab initio methods do not differ much then the described EFP charge separation may be induced by the full quantum methods up to some degree but will be offset by the now permitted charge transfer with the solvent. In order to estimate the charge transfers on each LiOH atom and on the whole LiOH molecule with H_2O molecules, the differences in the Mulliken charges $\Delta q_X = q_X^{RHF} - q_X^{EFP}$ between the RHF/6-311++G** and the EFP/RHF/6-311++G** methods for the species X = Li, O, H and LiOH in the $LiOH(H_2O)_n$ ($n = 1–6, 8$) clusters are listed in Table 8. Since the solute total charge in EFP is zero by model construction, Δq_{LiOH} measures directly the total charge interchanged between the whole LiOH molecule and the solvent at the RHF level that turns out to be always negative (net electrons gain). Data on Table 8 indicate that the dissociating isomers **6za** and **8za** display large LiOH electron transfers of 0.441 e^- and 0.377 e^- from the solvent, respectively, whereas most of the non-dissociating isomers exhibit LiOH electron transfers of 0.1 e^- to 0.2 e^-; exceptionally, the non-dissociating isomer **6j** shows a high LiOH electron transfer of 0.384 e^-. Therefore, the extent of solute/solvent charge

transfers in the $LiOH(H_2O)_n$ ($n = 1-6, 8$) clusters are considerable and their values are close to those found in the $Li^+(H_2O)_{1-6}$ ions by Merrill et al. [24]. The values of $\Delta q_H, \Delta q_O$ and Δq_{Li} measures the errors in the EFP atomic charge predictions with respect to RHF and those turn out to be negligible in the case of the H atom but considerable in the cases of the O and the Li atoms, specially in the latter. It is not possible to separate in this analysis the contributions of the solute internal charge redistribution and the solute charge transfer with the solvent to the values of Δq_X. However, it is reasonable to conclude that the individual Li and O atoms have significantly interchanged charge with the solvent, with Li taking electrons from and O giving electrons to the H_2O molecules. The total charge transfer on LiOH seems to be dominated by the large charge transfer on the Li atom. Although the LiOH solute at EFP/RHF/6-311++G** level has an incorrect charge distribution on its atoms and lacks the extra negative charge present in its full quantum counterparts, the agreement between this method and RHF/6-311++G** in structural properties such as Li–OH bond lengths and LiOH–H_2O distances can be deemed satisfactory. For instance, in the non- dissociating cases, the EFP and RHF Li–OH bond lengths differ by about 0.02 Å on average. In the dissociating cases correctly predicted by EFP, the agreement between the EFP and RHF Li–OH bond lengths is less satisfactory but still quite fair for a breaking bond. In some cases, the highest departures of the EFP Li–OH bond lengths from the RHF ones are correlated to high values of Δq_{LiOH} (e.g. isomers **6m**, **6n** and **8za**). Overall, the satisfactory agreement between EFP and RHF in the structural properties of the present study is in keeping with the findings by Merrill et al. [24], according to which EFP can still provide an accurate description of Li-bearing aqueous compounds in spite of extensive charge transfers. However, agreement in the relative energies ΔE is less satisfactory because some instances of conflicting orders in the clusters relative stabilities are observed. The ΔE values can be affected by charge-transfer processes. A more detailed analysis in terms of both the Morokuma–Kitaura [34] and the reduced variational space (RVS) [35] energy decompositions will single out the individual contribution of each energy component (Coulombic, polarization and exchange-charge transfer) to the overall accuracy of the present EFP calculations. Those analyses are postponed for future work.

At this point, it will be opportune to briefly compare the results of the present investigation on the LiOH base with the previous ones of its homologous NaOH base [5], especially in regard to some macroscopic properties of their bulk solutions. LiOH is noticeably less soluble in water (12.8 and 17.5 g per 100 cm^3 at 20 and 100 °C, respectively) than NaOH (42.0 and 347.0 g per 100 cm^3 at 0 and 100 °C, respectively) [36]. Although the basicity of LiOH and NaOH in aqueous solution at the same concentration are indistinguishable, gas-phase proton affinities experiments [37] show a lower basicity in the isolated LiOH molecule than in the NaOH one. Basic knowledge of inorganic chemistry indicates that the different chemical properties between the Li^+ and the Na^+ compounds are mostly a direct consequence of the differences between their ionic radii (0.90 and 1.16 Å, respectively [36]). In that regard, straightforward application of Fajans Rules [38] will predict a lesser ionic character in LiOH than in NaOH because of the smaller radius of Li^+. That decreased ionic character in LiOH should explain its lower aqueous solubility and lower gas-phase basicity. It was expected that a comparison of the main results of the present LiOH investigation with those of NaOH would perhaps provide a microscopic explanation for the macroscopic differences between the properties of LiOH and NaOH solutions. Although the solvation patterns of LiOH and NaOH show differences in detail, the present results for LiOH does not indicate that this base has a lesser propensity toward dissociation in aqueous clusters than NaOH. Particularly, an isolated LiOH molecule requires of six H_2O molecules to undergo its spontaneous dissociation as an isolated NaOH molecule does as well [5]. More drastic differences between the solvation behavior of LiOH and NaOH may probably be found if larger aqueous clusters are investigated.

Finally, it should be mentioned that there are not available experiential data for the $LiOH(H_2O)_n$ ($n = 1-6, 8$) clusters in the gas phase to compare the present results. However, an indirect comparison with some related experimental results will be discussed in Section 4.

4. Summary and conclusions

Solvation of the LiOH base in aqueous solutions at the microscopic level has not been studied theoretically until the present work. Geometry optimizations of the $LiOH(H_2O)_n$ ($n = 1-6, 8$) clusters were first calculated at the level of the EFP/RHF theory with the quantum LiOH molecule described by a RHF/6-311++G** wavefunction and with the classical H_2O molecules by the EFP model (EFP/RHF/6-311++G**); those EFP/RHF optimized geometries were used as the initial guesses for successive geometry optimizations with the RHF/6-311++G** and MP2/6-311++G** methods. Inspection of the structural properties calculated with the full quantum mechanics RHF/6-311++G** and MP2/6-311++G** methods clearly indicates that as the number of H_2O molecules added to the bare LiOH solute increases so does its Li–OH bond length with a concomitant decrease in the Li–OH bond order. This observed effect illustrates the progression of a single LiOH molecule toward its dissociation into a separated Li^+/OH^- ion pair in bulk solution. With these two full quantum mechanic methods, most of the calculated $LiOH(H_2O)_n$ ($n = 1-6, 8$) clusters contain a non-dissociated LiOH molecule within. However, in two calculated structures, the C_3-symmerty $LiOH(H_2O)_6$ isomer **6za** and the C_4-symmerty $LiOH(H_2O)_8$ isomer **8za**, the formation of

a separated Li^+/OH^- ion pair is observed at both the RHF/6-311++G** and MP2/6-311++G** levels. More importantly, the $LiOH(H_2O)_6$ isomer **6za** turns out to be the most stable structure in the $LiOH(H_2O)_6$ series of isomers at the MP2/6-311++G** level. This finding establishes that it is necessary to add at the least six H_2O molecules to a single LiOH molecule to provoke its spontaneous dissociation into a separated Li^+/OH^- ion pair in an aqueous cluster. On the contrary, the dissociated $LiOH(H_2O)_8$ isomer **8za** is not the most stable structure in the $LiOH(H_2O)_8$ series of isomers at both the RHF/6-311++G** and MP2/6-311++G** levels nor is the $LiOH(H_2O)_6$ isomer **6za** at the RHF/6-311++G** one in its corresponding series. An intermediate situation with a partially dissociated LiOH molecule is also observed in the $LiOH(H_2O)_3$ isomer **3a** at the MP2/6-311++G** level, which is the most stable structure in the $LiOH(H_2O)_3$ series. No direct experimental results on the $LiOH(H_2O)_n$ ($n = 1–6, 8$) clusters are available but comparisons with measurements on related species are possible. For instance, in the dissociated isomer **6za**, the dissociating OH^- group is coordinated with three H_2O molecules forming a nearly C_3-symmetry $OH^-(H_2O)_3$ moiety that is somewhat similar to the recently observed, first-solvation-shell, C_3-symmetry $OH^-(H_2O)_3$ cluster [2] in the gas phase. However, to make that dissociating moiety be exactly the same as the experimental $OH^-(H_2O)_3$ cluster, it would be necessary to rotate the three H_2O molecules around their axes along the $HOH–OH^-$ hydrogen bonds to place the three H atoms not involved in hydrogen bonding farther away from the OH^- group. Those conformational changes will spontaneously happen if the dissociating $OH^-(H_2O)_3$ moiety is farther removed from the cluster. On the contrary, in the isomer **8za**, the dissociating moiety is a nearly C_4-symmetry $OH^-(H_2O)_4$ ion, which will rearrange into a first-solvation-shell $OH^-(H_2O)_3$ cluster with an additional second-shell H_2O molecule [2] if farther removed from the cluster. Finally, in isomers **6za** and **8za**, the dissociating Li atom is not at the center of the cluster but in an apex position: the Li^+ ion dissociates carrying a few H_2O molecules on one side.

Inspection of the EFP/RHF/6-311++G** results for the whole $LiOH(H_2O)_n$ ($n = 1–6, 8$) series of clusters show a reasonable agreement with those done with the full quantum mechanics methods. At a qualitative level, the geometries, shapes and structural details of the calculated clusters display very similar features at the three levels of theory herein considered. At a quantitative level, the agreement between the EFP/RHF/6-311++G** and the RHF/6-311++G** methods is satisfactory in terms of structural properties (e.g. Li–OH bond lengths). This is expected because the EFP method was designed to reproduce closely the RHF results. However, the agreement in the relative energies ΔE at the EFP/RHF/6-311++G** and RHF/6-311++G** levels is less satisfactory because some instances of conflicting orders in the clusters relative stabilities are observed. It seems that the inclusion of electronic correlation in the MP2 method is crucial to predict some finer details of the dissociation process. For instance, both the EFP/RHF/6-311++G** and the RHF/6-311++G** calculations fail to reproduce the LiOH partial dissociation of the $LiOH(H_2O)_3$ isomer **3a** as the MP2/6-311++G** calculations do. More importantly, the RHF/6-311++G** method clearly predicts LiOH dissociation in the $LiOH(H_2O)_6$ isomer **6az** but that structure turned out not to be the most stable in the $LiOH(H_2O)_6$ series. As discussed in detail in Section 3.1.6, the EFP/RHF method applied to the calculation of that $LiOH(H_2O)_6$ isomer **6za** converge and correctly predict LiOH dissociation with the 6-31G, 6-31++G, 6-311G, 6-311G**, 6-311++G, 6-311++G(3df, 3pd) and cc-pVTZ basis sets; converges but fails to predict dissociation with the 6-311++G(2d, 2p) and 6-311++G(2df, 2pd) ones; and fail to converge with the 6-31G**, 6-31++G**, 6-311++G**, cc-pVDZ and STO-3G ones. Considering all the calculated $LiOH(H_2O)_6$ isomer **6za** structures in the present investigation, it can be seen that the instances of a converged EFP/RHF calculation with an accurate dissociation prediction in agreement with the full quantum mechanics results (seven cases) outnumber those converged calculations with an erroneous dissociation prediction (two cases). Currently, it is not possible to identify the reasons for that lack of convergence and/or for those converged but incorrect results. Most likely, the cause may lie in the delicate balance involving the intermolecular interactions between the EFP classical solvent and the quantum solute parts, including a basis set dependency from the latter. Only a careful numerical analysis of the implicated factors, including the Morokuma–Kitaura [34] and the reduced variational space (RVS) [35] energy decompositions, will reveal the origin of these two problems. However, it is very important to emphasize that those limitations encountered in a few EFP/RHF calculations are by no means insurmountable. Lack of convergence may be remedied by conditioning better the self-consistent RHF algorithms for an EFP use; and erroneous non-dissociating predictions may be corrected by re-parameterizing the internal EFP variables in the Coulombic, polarization and exchange-repulsion/charge-transfer interaction terms to deal with Li compounds. In fact, this investigation is one of the few applications of the EFP/RHF method to aqueous Li-bearing species after the pioneering EFP/RHF work by Merrill et al. on this type of compounds [24]. Finally, it should be noticed that the values of the Mulliken charges on the LiOH atoms at the EFP/RHF/6-311++G** level depart noticeably from those at the full quantum mechanics levels as a result of considerable solute–solvent charge transfers not accounted for by EFP. Fortunately, the conflicting EFP charge descriptions do not impede a reasonably agreement between the EFP/RHF/6-311++G** and RHF/6-311++G** methods in terms of structural properties (e.g. Li–OH bond lengths). In spite of a few discrepancies, the agreement

of the EFP/RHF method with the full ab initio calculations can be deemed satisfactory. Therefore, the present investigation gives further support to EFP as a reliable and feasible method to study solvation effects in relatively large aqueous clusters of ionic compounds.

Acknowledgements

The authors would like to express their gratitude to Prof. Mark S. Gordon and Dr Mike Schmidt (Iowa State University) for their helping discussions on the EFP method and the GAMESS program. All the present calculations have been completed at the Texas Tech University High Performance Computer Center (TTU HPCC), to which generous use of computer time and technical support are gratefully acknowledged. This research was supported in part by the Robert A. Welch Foundation grant D-1539 and by an award from Research Corporation. Also, acknowledgment is made to the donors of The American Chemical Society Petroleum Research Fund for partial support of this research.

References

[1] W.H. Robertson, M.A. Johnson, Science 298 (2002) 69.
[2] W.H. Robertson, E.G. Diken, E.A. Price, J.W. Shin, M.A. Johnson, Science 299 (2003) 1367.
[3] G.N. Patwari, J.M. Lisy, J. Chem. Phys. 118 (2003) 8555.
[4] O.M. Cabarcos, C.J. Weinheimer, J.M. Lisy, J. Chem. Phys. 110 (1999) 8429.
[5] A. Yoshikawa, P. Bandyopadhyay, M.S. Gordon, in preparation.
[6] P. Jungwirth, J. Phys. Chem. A 104 (2000) 145.
[7] C.P. Petersen, M.S. Gordon, J. Phys. Chem. A 103 (1999) 4162.
[8] D.E. Smith, L.X. Dang, J. Chem. Phys. 100 (1994) 3757.
[9] D.E. Woon, T.H. Dunning Jr, J. Am. Chem. Soc. 117 (1995) 1090.
[10] (a) T.H. Dunning Jr, J. Chem. Phys. 90 (1989) 1007. (b) R.A. Kendall, T.H. Dunning Jr, R.J. Harrison, J. Chem. Phys. 96 (1992) 6796. (c) D.E. Woon, T.H. Dunning Jr, J. Chem. Phys. 98 (1993) 1358.
[11] T. Asada, K. Nishimoto, Chem. Phys. Lett. 232 (1995) 518.
[12] K. Honda, K. Kitaura, Chem. Phys. Lett. 140 (1987) 53.
[13] K. Ando, J.T. Hynes, J. Mol. Liq. 64 (1995) 25.
[14] D.A. Estrin, J. Kohanoff, D.H. Laria, R.O. Weht, Chem. Phys. Lett. 280 (1997) 280.
[15] M.M. Szczesniak, S. Scheiner, Y. Bouteiler, J. Chem. Phys. 81 (1984) 5024.
[16] Z. Latajka, S. Sceiner, J. Chem. Phys. 87 (1987) 5928.
[17] L.G. Gorb, N.N. Il'chenko, V.V. Goncharuk, Russ. J. Phys. Chem. 65 (1991) 2418.
[18] C. Chipot, L.G. Gorb, J.L. Rivail, J. Phys. Chem. 98 (1994) 1601.
[19] M.J. Packer, D.C. Clary, J. Phys. Chem. 99 (1995) 14323.
[20] C. Lee, C. Sosa, M. Planas, J.J. Novoa, J. Chem. Phys. 104 (1996) 7081.
[21] S. Re, Y. Osamura, Y. Suzuki, H.F. Schafer, J. Chem. Phys. 109 (1998) 973.
[22] (a) P.N. Day, J.H. Jensen, M.S. Gordon, S.P. Webb, W.J. Stevens, M. Krauss, D. Garmer, H. Basch, D. Cohen, J. Chem. Phys. 105 (1996) 1968. (b) M.S. Gordon, M.A. Freitag, P. Bandyopadhyay, J.H. Jensen, V. Kairys, W.J. Stevens, J. Phys. Chem. A 105 (2001) 293.
[23] D. Kim, S. Hu, P. Tarakeshwar, K.S. Kim, J.M. Lisy, J. Phys. Chem. A 107 (2003) 1228.
[24] G.N. Merrill, S.P. Webb, D.B. Bivin, J. Phys. Chem. A 107 (2003) 386.
[25] D.J. Miklowitz, M.J. Goldstein, Bipolar Disorder, The Guilford Press, New York, 1997.
[26] G.N. Merrill, S.P. Webb, J. Phys. Chem. A 107 (2003) 7852.
[27] G.N. Merrill, S.P. Webb, J. Phys. Chem. A 108 (2004) 833.
[28] P. Bandyopadhyay, M.S. Gordon, J. Chem. Phys. 113 (2000) 1104.
[29] P. Bandyopadhyay, M.S. Gordon, B. Mennucci, J. Tomasi, J. Chem. Phys. 116 (2002) 5023.
[30] A.J. Stone, The Theory of Intermolecular Forces, Oxford University Press, New York, 1996.
[31] D.R. Garmer, W.J. Stevens, J. Phys. Chem. 93 (1989) 8263.
[32] M.W. Schmidt, K.K. Baldridge, J.A. Boatz, S.T. Elbert, M.S. Gordon, J.H. Jensen, K. Koseki, M. Matsunaga, K.A. Nguyen, S.J. Su, T.L. Windus, M. Dupuis, J.A. Montgomery, J. Comput. Chem. 14 (1993) 1347.
[33] M.J. Frisch, G.W. Trucks, H.B. Schlegel, G.E. Scuseria, M.A. Robb, J.R. Cheeseman, V.G. Zakrzewski, J.A. Montgomery, R.E. Stratmann, J.C. Burant, S. Dapprich, J.M. Millam, A.D. Daniels, K.N. Kudin, M.C. Strain, O. Farkas, J. Tomasi, V. Barone, M. Cossi, R. Cammi, B. Mennucci, C. Pomelli, C. Adamo, S. Clifford, J. Ochterski, G.A. Pettersson, P.Y. Ayala, Q. Cui, K. Morokuma, D.K. Malick, A.D. Rabuck, K. Raghavachari, J.B. Foresman, J. Cioslowski, J.V. Ortiz, B.B. Stefabov, G. Liu, A. Liashenko, P. Piskorz, I. Komoromi, R. Gomperts, R.L. Martin, D.J. Fox, T. Keith, A.L. Al-Laham, C.Y. Peng, A. Nanayakkara, C. Gonzalez, M. Head-Gordon, E.S. Replogle, J.A. Pople, GAUSSIAN 98, Pittsburgh PA, 1998.
[34] K. Kitaura, K. Morokuma, Int. J. Quantum Chem. 10 (1976) 325.
[35] (a) W.J. Stevens, W.H. Fink, Chem. Phys. Lett. 139 (1987) 15. (b) W. Chen, M.S. Gordon, J. Phys. Chem. 100 (1996) 14316.
[36] CRC Handbook of Chemistry and Physics, seventy fifth ed., CRC Press, Boca Raton, FL, 1994.
[37] H.L. Finston, A.C. Rychtman, A new view of the current acid-base theories, Wiley, New York, 1982.
[38] G.L. Miessler, D.A. Tarr, Inorganic Chemistry, Prince Hall, Englewood Cliffs, NJ, 1991.